

# Amplitude sensing below the zero-point fluctuations with a two-dimensional trapped-ion mechanical oscillator

K. A. Gilmore,<sup>1,2,\*</sup> J. G. Bohnet,<sup>1</sup> B. C. Sawyer,<sup>3</sup> J. W. Britton,<sup>4</sup> and J. J. Bollinger<sup>1,†</sup>

<sup>1</sup>*National Institute of Standards and Technology, Boulder, Colorado 80305, USA*

<sup>2</sup>*JILA and Department of Physics, University of Colorado, Boulder, Colorado, 80309, USA*

<sup>3</sup>*Georgia Tech Research Institute, Atlanta, Georgia 30332, USA*

<sup>4</sup>*U.S. Army Research Laboratory, Adelphi, Maryland 20783, USA*

(Dated: March 15, 2017)

We present a technique to measure the amplitude of a center-of-mass (COM) motion of a two-dimensional ion crystal composed of  $\sim 100$  ions in a Penning trap. By measuring motion at frequencies far from the oscillator resonance frequency, we resolve amplitudes as small as 50 pm, 40 times smaller than the COM mode zero-point fluctuations. The technique employs a spin-dependent, optical-dipole force to couple the mechanical oscillation to the electron spins of the trapped ions, enabling a discrete measurement of one quadrature of the COM motion through a readout of the spin state. We demonstrate sensitivity limits set by spin-projection noise and spin decoherence due to off-resonant light scattering. When performed on resonance with the COM mode frequency, the technique demonstrated here can enable the detection of extremely weak forces ( $< 1$  yN) and electric fields ( $< 1$  nV/m), providing an opportunity to probe quantum sensing limits and search for physics beyond the standard model.

Measuring the amplitude of mechanical oscillators has engaged physicists for more than 50 years [1, 2] and, as the limits of amplitude sensing have dramatically improved, produced exciting advances both in fundamental physics and in applied work. Examples include the detection of gravitational waves [3], the coherent quantum control of mesoscopic objects [4], improved force microscopy [5], and the transduction of quantum signals [6]. During the past decade, optomechanical systems have facilitated increasingly sensitive techniques for reading out the amplitude of a mechanical oscillator [7–11], with a recent demonstration obtaining a measurement imprecision more than two orders of magnitude below the size of the ground state wave function (i.e. the amplitude  $z_{ZPT}$  of the zero-point fluctuations) [12]. While optomechanical systems have assumed a wide range of physical systems, including toroidal resonators, nanobeams, membranes and others, the basic principle involves coupling the amplitude of a mechanical oscillator to the resonant frequency of an optical cavity mode [4].

Crystals of laser-cooled, trapped ions behave as atomic-scale mechanical oscillators [13–15] with tunable oscillator modes and high quality factors ( $\sim 10^6$ ). Furthermore, laser cooling enables ground state cooling and non-thermal state generation of these oscillators. Trapped-ion crystals therefore provide an ideal experimental platform for investigating the fundamental limits of amplitude sensing, but to date there have only been a handful of investigations [14–17]. References [14–16] demonstrate the detection of amplitudes larger than the zero-point fluctuations of the trapped ion oscillator, while [17] reports on injection locking of optically excited mechanical oscillations of a single trapped ion seeded by a weak drive.

In this Letter we experimentally and theoretically an-

alyze a technique to measure the center-of-mass (COM) motion of a two-dimensional, trapped-ion crystal of  $\sim 100$  ions with a sensitivity below  $z_{ZPT}$ . We employ a time-varying spin-dependent force  $F_0 \cos(\mu t)$  that couples the amplitude of the COM motion with the internal spin degree of freedom of the ions [18, 19]. When the frequency  $\mu$  matches the frequency  $\omega$  of an imposed COM oscillation,  $Z_c \cos(\omega t)$ , spin precession proportional to  $Z_c$  occurs, which we read out at the end of the measurement with a precision imposed by spin projection noise [20]. The amplitude dependent spin precession is analogous to the optomechanical frequency shift of a cavity mode.

Our technique provides a discrete measurement of a single quadrature of the COM motion sensed during the application of the spin-dependent force. To determine the read-out imprecision in a regime free from thermal noise, we perform measurements where  $\omega$  is far from resonance with the trap axial frequency  $\omega_z$ . Additionally, we implement a protocol where the phase of the measured quadrature randomly varies from one realization of the experiment to the next, appropriate for sensing a force whose phase is unknown or not stable. For  $N = 85$  ions and  $z_{ZPT} \equiv \frac{1}{\sqrt{N}} \sqrt{\frac{\hbar}{2m\omega_z}} \approx 2$  nm, we detect amplitudes  $Z_c = 500$  pm in a single measurement and as small as 50 pm with 16 s of integration.

Our experimental apparatus, described in Fig. 1 and [18, 21], consists of  $N \sim 100$   $^9\text{Be}^+$  ions laser-cooled to the Doppler limit of 0.5 mK and confined to a single-plane Coulomb crystal in a Penning trap. The spin-1/2 degree of freedom is the  $^2S_{1/2}$  ground-state valence electron spin  $|\uparrow\rangle (|\downarrow\rangle) \equiv |m_s = +1/2\rangle (|m_s = -1/2\rangle)$ . In the magnetic field of the Penning trap, the ground state is split by 124 GHz. A resonant microwave source is used to perform global rotations of the spin ensemble. A pair of laser beams, detuned from the nearest optical transitions

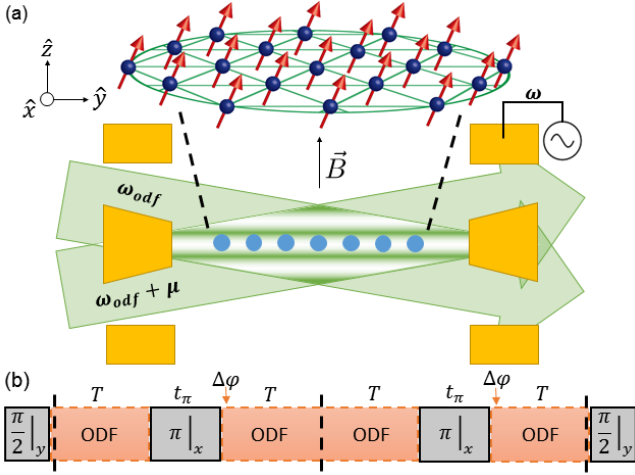


FIG. 1. (a) Representation of ion spins arranged in a 2D triangular lattice, along with a cross-sectional illustration of the Penning trap, characterized by an axial magnetic field  $B = 4.45$  T and an axial trap frequency  $\omega_z = 2\pi \times 1.57$  MHz. The blue dots represent ions. Cylindrical electrodes (yellow) generate a harmonic confining potential along the  $\hat{z}$ -axis. Radial confinement is provided by the Lorentz force from  $\vec{E} \times \vec{B}$ -induced rotation in the axial magnetic field. The beams generating the spin-dependent optical dipole force (green arrows) cross the ion plane at  $\pm 10^\circ$ , forming a 1D traveling-wave potential (green lines) with a  $0.9 \mu\text{m}$  wavelength. An AC voltage source is connected to the trap endcap and used to drive an axial oscillation with calibrated amplitude  $Z_c$ . (b) Quantum lock-in CPMG sequence used to detect spin precession produced by COM motion resonant with the ODF. Doppler cooling and  $|\uparrow\rangle_N$  spin state preparation occur before the sequence, and spin state detection after. Grey blocks with solid borders represent microwave  $\pi/2$  rotations about  $\hat{y}$  and  $\pi$  rotations about  $\hat{x}$ . Orange blocks with dashed borders represent ODF pulses. The ODF phase is advanced by  $\Delta\varphi$  in a modulation scheme discussed in [22], where  $\Delta\varphi = \pi$  for  $\omega = \mu$ . Dashed lines indicate the  $m$  segments of the sequence, here  $m = 2$ . We make use of an  $m = 8$  sequence for Figs. (2)-(4).

by  $\sim 20$  GHz, interfere to form a one-dimensional (1D) traveling-wave potential. The resulting spin-dependent optical dipole force (ODF) couples the spins to the ions' axial motion. Optical pumping prepares the initial state  $|\uparrow\rangle_N \equiv |\uparrow\uparrow\cdots\uparrow\rangle$  with high fidelity. At the end of the experiments described here we measure the probability  $P_\uparrow$  for an ion spin to be in  $|\uparrow\rangle$  from a global measurement of state-dependent resonance fluorescence on the Doppler cooling transition, where spin  $|\uparrow\rangle$  ( $|\downarrow\rangle$ ) is bright (dark).

The ODF couples the spin and motional degrees of freedom through the interaction [21]

$$\hat{H}_{ODF} = F_0 \cos(\mu t) \sum_i \hat{z}_i \hat{\sigma}_i^z, \quad (1)$$

where  $F_0 = U \delta k DWF$  is the magnitude of the ODF,  $\mu$  is the frequency difference between the ODF beams, and  $\hat{z}_i$  and  $\hat{\sigma}_i^z$  are the position operator and Pauli spin matrix for ion  $i$ . Here  $U$  ( $\delta k$ ) is the zero-to-peak poten-

tial (wave vector) of the 1D traveling-wave. The term  $DWF = \exp(-\delta k^2 \langle \hat{z}_i^2 \rangle / 2)$  is the Debye-Waller factor, a reduction in interaction strength due to the departure from the Lamb-Dicke confinement regime [23]. We estimate  $DWF \approx 0.86$  for the 0.5 mK Doppler laser cooling limit. The potential  $U$ , and therefore  $F_0$ , is determined from AC Stark shift measurements on the ions [24]. Typical maximum values for this work are  $U/\hbar \simeq 2\pi \times (10.4 \text{ kHz})$  resulting in  $F_0 \simeq 40 \text{ yN}$ .

With a weak RF drive on a trap electrode (see Fig. 1(a)) at a frequency  $\omega$  far from  $\omega_z$ , we impose a weak, classically driven COM motion of constant amplitude and phase,  $\hat{z}_i \rightarrow \hat{z}_i + Z_c \cos(\omega t + \delta)$ . With  $\delta k Z_c \ll 1$  and assuming  $\mu \sim \omega$ , we use Eq. (1) to describe the shift in the spin transition frequency due to the coherent amplitude  $Z_c$ ,

$$\hat{H}_{ODF} = F_0 Z_c \cos((\omega - \mu)t + \delta) \sum_i \frac{\hat{\sigma}_i^z}{2}. \quad (2)$$

For  $\mu = \omega$  there is a static shift  $\Delta(Z_c)$  in the frequency of the spin transition,  $\Delta(Z_c) = (F_0/\hbar) Z_c \cos(\delta)$ .

We measure  $\Delta(Z_c)$  from the resulting spin precession in an experiment like that shown in Fig. 1(b). Ideally, spin precession can be measured using a Ramsey-type experiment where the ions are prepared in the  $|\uparrow\rangle_N$  state, followed by a microwave  $\pi/2$  pulse about  $\hat{y}$  that rotates the spins to the  $\hat{x}$  axis. The spins are then allowed to precess for an interaction time  $\tau$  so that the resulting spin precession on resonance ( $\mu = \omega$ ) is  $\theta = \theta_{max} \cos(\delta)$  where  $\theta_{max} \equiv (F_0/\hbar) Z_c \tau$ . After a final  $\pi/2$  pulse about  $\hat{y}$ , the final state readout measures the population of the spins in  $|\uparrow\rangle$ ,  $P_\uparrow = \frac{1}{2}[1 - e^{-\Gamma\tau} \cos(\theta)]$ . Here  $\Gamma$  is the decay rate from spontaneous emission from the off-resonant ODF laser beams [25]. To detect small amplitudes with the available  $F_0$  in our set-up, we extend the spin-precession time to  $\tau \geq 20 \text{ ms}$  ( $T \geq 1.25 \text{ ms}$ , in Fig. 1(b)). To avoid decoherence due to magnetic field fluctuations and coherently accumulate spin precession, we use a quantum lock-in [26] sequence where during the interaction time  $\tau$  the spin precession is interrupted by a train of  $\pi$ -pulses that are synchronized with phase jumps enforced on the ODF beams [22]. In particular, we use a Carr-Purcell-Meiboom-Gill (CPMG) sequence with  $m = 8$  ODF- $\pi$ -ODF segments (see Fig. 1(b)).

We allow the phase  $\delta$  to randomly vary from one realization of the experiment to the next, effectively measuring a random quadrature of the motion each measurement trial. Such a scheme is relevant for sensing a force with an unknown or unstable phase. Different experimental trials therefore result in a different precession  $\theta$ , as indicated in Fig. 3. We measure the collective dephasing (or decoherence) using  $\langle P_\uparrow \rangle = \frac{1}{2}[1 - e^{-\Gamma\tau} \langle \cos(\theta) \rangle]$ , where the brackets  $\langle \cdot \rangle$  denote an average over many measurements. Averaging over the random phase  $\delta$  yields

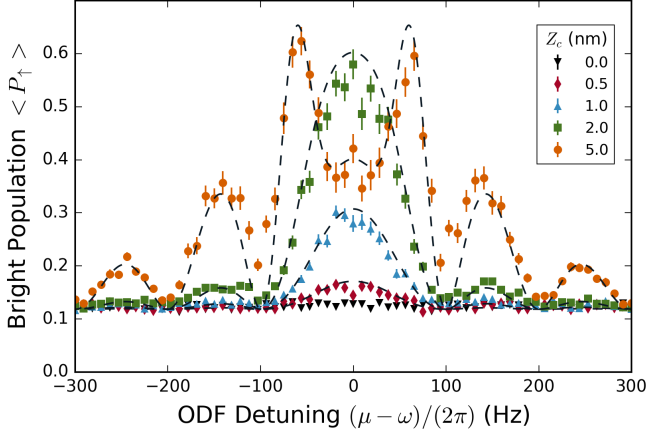


FIG. 2. Lineshape of the spin precession signal for amplitudes  $Z_c$  of 500 pm (red diamonds), 1 nm (blue triangles), 2 nm (green squares), and 5 nm (orange circles) for  $\tau = 20$  ms. Black triangles are the background, with the drive turned off. Dashed lines are theoretical predictions with no free parameters. Error bars represent standard error. Here  $N = 90$  ions and  $F_0 = 7.9$  yN.

[27]

$$\langle P_{\uparrow} \rangle = \frac{1}{2} [1 - e^{-\Gamma\tau} J_0(\theta_{max})]. \quad (3)$$

Here  $J_0$  is the zeroth order Bessel function of the first kind.

To create the steady-state COM axial oscillation  $Z_c \cos(\omega t + \delta)$ , we applied a continuous AC voltage to an endcap of the Penning trap at a frequency  $\omega/(2\pi)$  near 400 kHz. This frequency was chosen because it was far from any motional mode frequencies of the ion crystal, and there were no observed sources of noise. Thus, the background, i.e. the signal without the driven COM axial motion, was fully characterized by decoherence due to spontaneous emission and is given by  $\langle P_{\uparrow} \rangle_{bck} = \frac{1}{2} [1 - e^{-\Gamma\tau}]$ . We calibrated the displacement of the ions due to a static voltage applied to the endcap by measuring the resulting movement of the ion crystal in the side-view imaging system. From this calibration, we determined that a 1 V offset results in a  $0.97(5)$   $\mu\text{m}$  displacement of the ions. We estimate that the corrections for using this DC calibration to estimate  $Z_c$  for an  $\omega/(2\pi) \approx 400$  kHz drive is less than 10 %.

Figure 2 shows the emergence of the measured spin precession signal out of the background as the amplitude  $Z_c$  is increased from 500 pm to 5 nm. The measured lineshape agrees well with the prediction, detailed in [22], involving no free parameters.

Figure 3 shows the background and the measured resonant ( $\mu = \omega$ ) response to a fixed  $Z_c = 485$  pm oscillation for a range of ODF strengths  $F_0/F_{0M}$ , where  $F_{0M}$  is the maximum  $F_0$  possible with our current set-up ( $\sim 40$  yN). Agreement with Eq. (3) involving no free parameters is

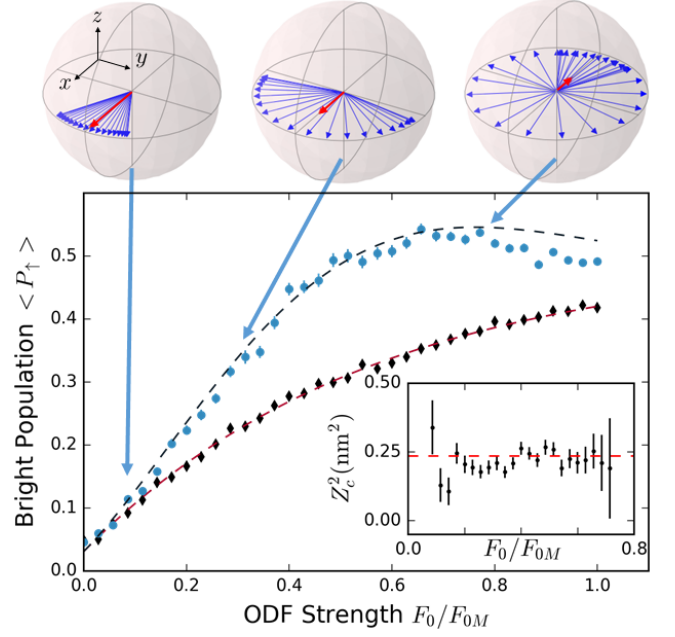


FIG. 3. **Top:** Bloch sphere representation [28] of spin dephasing for  $Z_c = 485$  pm. Each blue vector represents an experimental trial with a different phase  $\delta$  (see text). From left to right, the spread in the blue vectors corresponds to  $\theta_{max} = 0.470, 1.41, 3.62$  radians and  $F_0/F_{0M} = 0.1, 0.3, 0.77$ , where  $F_{0M}$  is the maximum optical-dipole force. Our experiment measures the length of the Bloch vector averaged over many trials, denoted by the thick red vector. **Main plot:** As a function of ODF strength, the background (black diamonds) with no applied drive and signal (blue points) for a 485 pm amplitude and total ODF interaction time  $\tau = 24$  ms is shown. The red dashed line is a fit to the background. The black dashed line is the theoretical prediction with no free parameters, given the background fit. Here  $N = 75$  ions and  $F_{0M} = 41.3$  yN. **Inset:** Black points are experimentally determined values for  $Z_c^2$ . Red dashed line is the calibrated value of  $Z_c^2$ . Error bars represent standard error.

excellent. For both Figs. 2 and 3 the background is within 6 % of that determined by independent measurements of the spontaneous emission decay rates of each ODF beam [24]. The amplitude  $Z_c = \theta_{max}/(\tau F_0/\hbar)$  can be determined from the difference  $\langle P_{\uparrow} \rangle - \langle P_{\uparrow} \rangle_{bck}$ . We note that  $\langle P_{\uparrow} \rangle - \langle P_{\uparrow} \rangle_{bck}$  depends on  $\theta_{max}^2$ . Therefore, the sensing protocol described here directly measures  $Z_c^2$ . The inset of Fig. 3 shows a determination of  $Z_c^2$  as the power in the ODF beams is increased. The uncertainties were determined from the measured noise of the  $\langle P_{\uparrow} \rangle - \langle P_{\uparrow} \rangle_{bck}$  measurements using standard error propagation [22]. These uncertainties go through a minimum, indicating an optimum  $F_0/F_{0M}$  value for the determination of  $Z_c^2$ .

To explore the ultimate amplitude sensing limits of our protocol, we performed repeated pairs of  $P_{\uparrow}$  measurements, first with  $Z_c = 0$  (i.e. no off-resonant drive on the trap endcap) to get the background, and then with  $Z_c \neq$

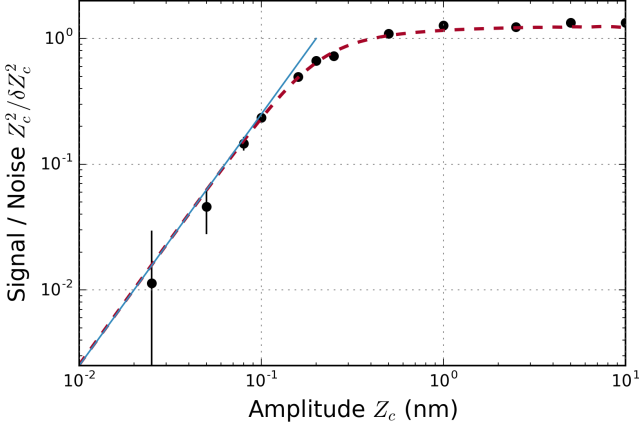


FIG. 4. Amplitude sensing limits for  $N = 85$ . Black points are experimentally determined values of signal-to-noise for single measurements of  $Z_c^2$  as a function of the experimentally imposed  $Z_c$ . Our measurement for  $Z_c = 25$  pm is consistent with zero. The red dashed line is the theoretical prediction for the signal-to-noise including projection noise and the random COM mode quadrature measured each trial. Blue solid line is the predicted limiting signal-to-noise for small amplitudes (Eq. (5)), assuming only projection noise and parameters relevant for our set-up. Error bars represent standard error.

0. For a given  $Z_c$ , 3,000 pairs of measurements were used to determine the average difference  $\langle P_\uparrow \rangle - \langle P_\uparrow \rangle_{bck}$  and the standard deviation  $\sigma(P_\uparrow - P_{\uparrow,bck})$  of the difference for a single pair of measurements. For each  $Z_c$ ,  $F_0/F_{0M}$  was set close to the value that maximizes the signal-to-noise ratio of the  $Z_c^2$  determination. This occurs for relatively small  $\theta_{max}$  such that  $\frac{1}{2}(1 - J_0(\theta_{max})) \approx \theta_{max}^2/8$ . Then, the signal-to-noise ratio of a determination of  $Z_c^2$  from a single pair of  $P_\uparrow$ ,  $P_{\uparrow,bck}$  measurements is approximately

$$\frac{Z_c^2}{\delta Z_c^2} \approx \frac{\langle P_\uparrow \rangle - \langle P_\uparrow \rangle_{bck}}{\sigma(P_\uparrow - P_{\uparrow,bck})}. \quad (4)$$

Figure 4 displays Eq. (4) from measurements acquired with  $Z_c$  ranging from 10 nm to as small as 0.025 nm. Excellent agreement is observed with a model (dashed red line) that assumes the only sources of noise are projection noise in the spin state detection and fluctuations in  $P_\uparrow$  produced by random variation in the phase  $\delta$  between the COM motion and the ODF from one measurement to the next.

For amplitudes  $Z_c \gtrsim 500$  pm, noise due to different realizations of the phase  $\delta$  dominates. This situation is depicted by the middle Bloch sphere of Fig. 3. The fluctuations in  $P_\uparrow$  due to different realizations of  $\delta$  are comparable to the signal  $\langle P_\uparrow \rangle - \langle P_\uparrow \rangle_{bck}$ , limiting the signal-to-noise of a single measurement of  $Z_c^2$  to  $\sim 1$ . As  $Z_c$  decreases, this noise and the signal decrease while projection noise stays approximately the same, resulting in a decreasing  $Z_c^2/\delta Z_c^2$ . For small  $Z_c$ , we show the sensitivity

is determined by  $N$ ,  $\delta k$ , and the ratio of the spontaneous decay rate to the optical potential  $\xi \equiv \Gamma/(U/\hbar)$  [22], according to

$$\left. \frac{Z_c^2}{\delta Z_c^2} \right|_{\text{limiting}} \approx 0.097 \frac{\sqrt{N}(DWF)^2(\delta k)^2}{\xi^2} Z_c^2. \quad (5)$$

For  $N = 85$  and values of  $DWF$ ,  $\delta k$ , and  $\xi = 1.156 \times 10^{-3}$  relevant for our set-up,  $Z_c^2/\delta Z_c^2 \approx [Z_c/0.2 \text{ nm}]^2$ , displayed as the blue line in Fig. 4. On the log-log plot the slope of 2 is the result of a signal proportional to  $Z_c^2$  along with a constant readout noise of the spins (here projection noise). We perform 16 measurements in 1 s, so the single measurement  $Z_c^2/\delta Z_c^2 \approx [Z_c/0.2 \text{ nm}]^2$  corresponds to a long averaging time sensitivity of  $(100 \text{ pm})^2/\sqrt{\text{Hz}}$  (recall that our protocol measures  $Z_c^2$ ).

Figure 4 documents a good understanding of the sensing limits of our protocol, indicating how the measurement can be improved in the future. Equation (5) scales as  $1/\xi^2$ , resulting in significant improvements for set-ups with less spontaneous decay. By stabilizing the ODF beatnote phase with respect to the classical drive [29, 30], or performing measurements conditioned on a pre-measurement designed to identify the relative phase between the ODF and classical drive, we could repeatedly measure the same quadrature of motion and realize a substantial improvement in sensitivity. For this phase-coherent protocol, we estimate [22] a single measurement imprecision of 74 pm for  $N = 100$  and current parameters of our set-up, almost 30 times smaller than the zero-point fluctuations, producing a long averaging time sensitivity of  $\sim 18 \text{ pm}/\sqrt{\text{Hz}}$ . The use of spin-squeezed states, recently demonstrated in this system [21], can provide an additional enhancement by reducing the projection noise of the readout.

The 50 pm amplitude detected in Fig. 4 at a frequency  $\omega$  far from resonance corresponds to an electric field detection of 0.46 mV/m or 73 yN/ion. These force and electric field sensitivities can be improved by the  $Q$  of the COM mode by probing near resonance with  $\omega_z$ . Quality factors  $Q \sim 10^6$  should be possible with trapped-ion COM modes. The detection of a 20 pm amplitude resulting from a 100 ms coherent drive on the 1.57 MHz COM mode is sensitive to a force/ion of  $5 \times 10^{-5}$  yN corresponding to an electric field of 0.35 nV/m. Probing on resonance with a sensitivity below the zero-point fluctuations requires a protocol that evades back action due to coupling to thermal and quantum fluctuations [31]. Electric field sensing below  $\sim 0.1$  nV/m provides an opportunity to search for hidden photon dark matter [32, 33], although shielding effects must be carefully considered. Ion traps typically operate with frequencies  $\omega_z$  in the 50 kHz to 5 MHz range, providing a sensitivity to hidden photon masses in the  $2 \times 10^{-10}$  eV to  $2 \times 10^{-8}$  eV range.

In summary, we have presented a technique for amplitude sensing below the zero-point fluctuations of a

trapped ion mechanical oscillator. By coupling the spin and motional degrees of freedom of the ions, a single quadrature of the motional state of the ions may be sensitively read out. We implement a protocol where the phase of the measured quadrature randomly varies, detecting a 500 pm amplitude in a single measurement and demonstrating a long measurement time sensitivity of  $(100 \text{ pm})^2 / \sqrt{\text{Hz}}$ . Modifications of our set-up should enable repeated measurements of a single quadrature, resulting in a single measurement imprecision of 74 pm for  $N = 100$  ions, providing opportunities for trapped ion mechanical oscillators to explore the quantum limits of amplitude and force sensing, and enable new tools in the search for physics beyond the standard model.

We thank V. Sudhir, R. Ozeri, S. Kotler, and J. Teufel for stimulating discussions. K.G. is supported by NSF grant PHY 1521080. This manuscript is a contribution of NIST and not subject to U.S. copyright.

---

\* kevin.gilmore@colorado.edu

† john.bollinger@nist.gov

- [1] J. Weber, *Physical Review Letters* **17**, 1228 (1966).
- [2] C. M. Caves, *Physical Review Letters* **45**, 75 (1980).
- [3] B. P. Abbott *et al.* (LIGO Scientific Collaboration and Virgo Collaboration), *Physical Review Letters* **116**, 061102 (2016).
- [4] M. Aspelmeyer, T. J. Kippenberg, and F. Marquardt, *Reviews of Modern Physics* **86**, 1391 (2014).
- [5] H.-J. Butt, B. Cappella, and M. Kappl, *Surface Science Reports* **59**, 1 (2005).
- [6] T. A. Palomaki, J. W. Harlow, J. D. Teufel, R. W. Simmonds, and K. W. Lehnert, *Nature* **495**, 210 (2013).
- [7] J. D. Teufel, T. Donner, M. A. Castellanos-Beltran, J. W. Harlow, and K. W. Lehnert, *Nature Nanotechnology* **4**, 820 (2009).
- [8] G. Anetsberger, O. Arcizet, Q. P. Unterreithmeier, R. Rivière, A. Schliesser, E. M. Weig, J. P. Kotthaus, and T. J. Kippenberg, *Nature Physics* **5**, 909 (2009).
- [9] T. Westphal, D. Friedrich, H. Kaufer, K. Yamamoto, S. Gößler, H. Müller-Ebhardt, S. L. Danilishin, F. Y. Khalili, K. Danzmann, and R. Schnabel, *Physical Review A* **85**, 063806 (2012).
- [10] S. Schreppler, N. Spethmann, N. Brahms, T. Botter, M. Barrios, and D. M. Stamper-Kurn, *Science* **344**, 1486 (2014).
- [11] N. S. Kampel, R. W. Peterson, R. Fischer, P. L. Yu, K. Cicak, R. W. Simmonds, K. W. Lehnert, and C. A. Regal, *Physical Review X* (2017), arXiv:1607.06831.
- [12] D. J. Wilson, V. Sudhir, N. Piro, R. Schilling, a. Ghadimi, and T. J. Kippenberg, *Nature* **524**, 325 (2014).
- [13] J. D. Jost, J. P. Home, J. M. Amini, D. Hanneke, R. Ozeri, C. Langer, J. J. Bollinger, D. Leibfried, and D. J. Wineland, *Nature* **459**, 683 (2009).
- [14] M. J. Biercuk, H. Uys, J. W. Britton, A. P. VanDevender, and J. J. Bollinger, *Nature Nanotechnology* **5**, 646 (2010).
- [15] B. C. Sawyer, J. W. Britton, A. C. Keith, C.-C. J. Wang, J. K. Freericks, H. Uys, M. J. Biercuk, and J. J. Bollinger, *Physical Review Letters* **108**, 213003 (2012).
- [16] R. Shaniv and R. Ozeri, *Nature Communications* **8**, 14157 (2017).
- [17] S. Knünz, M. Herrmann, V. Batteiger, G. Saathoff, T. W. Hänsch, K. Vahala, and T. Udem, *Physical Review Letters* **105**, 013004 (2010).
- [18] B. C. Sawyer, J. W. Britton, and J. J. Bollinger, *Physical Review A* **89**, 033408 (2014).
- [19] P. A. Ivanov, *Physical Review A* **94**, 022330 (2016).
- [20] W. M. Itano, J. C. Bergquist, J. J. Bollinger, J. M. Gilligan, D. J. Heinzen, F. L. Moore, M. G. Raizen, and D. J. Wineland, *Physical Review A* **47**, 3554 (1993).
- [21] J. G. Bohnet, B. C. Sawyer, J. W. Britton, M. L. Wall, A. M. Rey, M. Foss-Feig, and J. J. Bollinger, *Science* **352**, 1297 (2016).
- [22] See Supplemental Material for technical details and derivations.
- [23] D. J. Wineland, C. Monroe, W. M. Itano, D. Leibfried, B. E. King, and D. M. Meekhof, *Journal of Research of the National Institute of Standards and Technology* **103**, 259 (1998).
- [24] J. W. Britton, B. C. Sawyer, A. C. Keith, C.-C. J. Wang, J. K. Freericks, H. Uys, M. J. Biercuk, and J. J. Bollinger, *Nature* **484**, 489 (2012).
- [25] H. Uys, M. J. Biercuk, a. P. Vandevender, C. Ospelkaus, D. Meiser, R. Ozeri, and J. J. Bollinger, *Physical Review Letters* **105**, 200401 (2010).
- [26] S. Kotler, N. Akerman, Y. Glickman, A. Keselman, and R. Ozeri, *Nature* **473**, 61 (2011).
- [27] S. Kotler, N. Akerman, Y. Glickman, and R. Ozeri, *Physical Review Letters* **110**, 110503 (2013).
- [28] J. R. Johansson, P. D. Nation, and F. Nori, *Computer Physics Communications* **183**, 1760 (2012).
- [29] D. B. Hume, C. W. Chou, D. R. Leibbrandt, M. J. Thorpe, D. J. Wineland, and T. Rosenband, *Physical Review Letters* **107**, 243902 (2011).
- [30] M. J. Biercuk, H. Uys, J. W. Britton, a. P. Vandevender, and J. J. Bollinger, *Optics Express* **19**, 10304 (2011).
- [31] C. Hempel, B. P. Lanyon, P. Jurcevic, R. Gerritsma, R. Blatt, and C. F. Roos, *Nature Photonics* **7**, 630 (2013).
- [32] P. Arias, D. Cadamuro, M. Goodsell, J. Jaeckel, J. Redondo, and A. Ringwald, *Journal of Cosmology and Astroparticle Physics* **2012**, 013 (2012).
- [33] S. Chaudhuri, P. W. Graham, K. Irwin, J. Mardon, S. Rajendran, and Y. Zhao, *Physical Review D* **92**, 075012 (2015).

# Supplemental Material: Amplitude sensing below the zero-point fluctuations with a two-dimensional trapped-ion mechanical oscillator

K. A. Gilmore,<sup>1,2,\*</sup> J. G. Bohnet,<sup>1</sup> B. C. Sawyer,<sup>3</sup> J. W. Britton,<sup>4</sup> and J. J. Bollinger<sup>1,†</sup>

<sup>1</sup>*National Institute of Standards and Technology, Boulder, Colorado 80305, USA*

<sup>2</sup>*JILA and Department of Physics, University of Colorado, Boulder, Colorado, 80309, USA*

<sup>3</sup>*Georgia Tech Research Institute, Atlanta, Georgia 30332, USA*

<sup>4</sup>*U.S. Army Research Laboratory, Adelphi, Maryland 20783, USA*

## INTRODUCTION

In this supplemental material we provide detailed derivations for a number of theoretical formulas and results of the main text. Specifically, in the first section we derive the shift in the spin transition frequency due to the coherent amplitude  $Z_c$  (Eq. (2) of the main text) from a more basic perspective. We also discuss in detail our modulation scheme. In the second section we derive the lineshape function used in Fig. 2 of the main text. In section 3 we describe the formalism used to determine the optimum signal-to-noise ratio for a measurement of  $Z_c^2$ . We used this optimum signal-to-noise ratio to generate the theoretical curve in Fig. 4 of the main text. We also derive the sensitivity limits for phase-incoherent amplitude sensing, where the phase difference between the driven motion and the ODF randomly varies from one realization of the experiment to the next. We show how these limits depend on  $\Gamma/(U/\hbar)$ ,  $\delta k$ , and  $N$ . Finally, in section 4 we consider the amplitude sensing limits assuming phase coherence between the spin-dependent force and the driven amplitude.

## CONTENTS

Introduction	2
1. Shift in the spin transition frequency, and the modulation scheme	2
2. Lineshape	3
3. Phase-incoherent sensing limits	5
4. Phase-coherent sensing limits	6
References	7

### 1. SHIFT IN THE SPIN TRANSITION FREQUENCY, AND THE MODULATION SCHEME

Figure 1 shows the Carr-Purcell-Meiboom-Gill (CPMG) sequence used to apply the 1D traveling-wave potential. The interaction of the spin degree of freedom with the 1D traveling-wave potential is given by

$$\hat{H}_{ODF} = U \sum_i \sin(\delta k \cdot \hat{z}_i - \mu t + \phi) \hat{\sigma}_i^z = U \sum_i \sin(\delta k \cdot \hat{z}_i) \cos(\mu t - \phi) \hat{\sigma}_i^z - U \sum_i \cos(\delta k \cdot \hat{z}_i) \sin(\mu t - \phi) \hat{\sigma}_i^z. \quad (1)$$

Here we explicitly include a phase  $\phi$  for the traveling-wave potential. Without loss of generality, we assumed  $\phi = 0$  in the main text. If  $\delta k \langle \hat{z}_i \rangle \ll 1$ , then  $\langle \cos(\delta k \cdot \hat{z}_i) \rangle \sim 1$ , and the spin precession due to the second term will be bounded by  $(U/\hbar)/\mu$ .

Typically,  $(U/\hbar)/\mu \ll 1$  and thus this term is ignored in most treatments. At low frequencies  $\mu \leq U/\hbar$  this term could be important, but it may be canceled by advancing the phase of the ODF by  $\Delta\phi = \mu(T + t_\pi)$  at each microwave  $\pi$ -pulse of the CPMG sequence (see Fig. 1). When  $\mu/2\pi = (2n + 1)/(2(T + t_\pi))$  for some integer  $n$ ,  $\Delta\phi = \pi$  and we recover the quantum lock-in phase advance of [1]. This phase advance coherently accumulates spin precession from the first term of Eq. (1) when  $\omega/2\pi = (2n + 1)/(2(T + t_\pi))$ . The term that survives our modulation scheme is

$$\hat{H}_{ODF} \simeq U \sum_i \sin(\delta k \cdot \hat{z}_i) \cos(\mu t - \phi) \hat{\sigma}_i^z. \quad (2)$$

We now impose a weak, classically driven COM motion of constant amplitude and phase  $\hat{z}_i \rightarrow \hat{z}_i + Z_c \cos(\omega t + \delta)$ . This can be thought of as the center of the Penning trap being moved by  $\pm Z_c$  at a frequency  $\omega$  far from the trap axial frequency  $\omega_z$ . With  $\delta k Z_c \ll 1$ , we obtain

$$\hat{H}_{ODF} \simeq U \sum_i (\delta k Z_c \cos(\delta k \cdot \hat{z}_i) \cos(\omega t + \delta) \cos(\mu t - \phi) + \sin(\delta k \cdot \hat{z}_i) \cos(\mu t - \phi)) \hat{\sigma}_i^z. \quad (3)$$

The second term of Eq. (3) is the usual term that gives rise to spin-motion entanglement with the drumhead modes and to effective spin-spin interactions [2, 3]. We assume we can neglect this term because we tune  $\mu$  far from any drumhead modes.



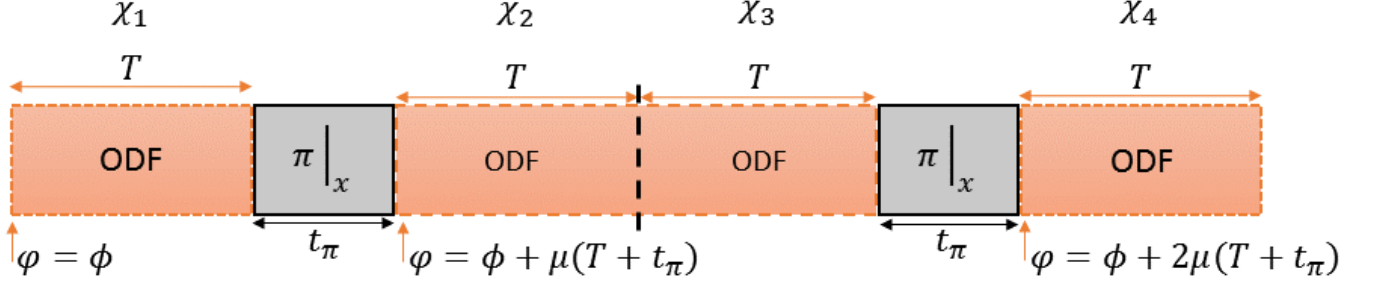


FIG. 1.  $m = 2$  CPMG sequence with total ODF interaction time  $4T$ .  $\varphi$  is the phase of the ODF beatnote. The  $\chi_i$  labels represent the periods over which the accumulated phase is considered in the text.

Deep in the Lamb-Dicke confinement regime, the  $\cos(\delta k \cdot \hat{z}_i)$  factor in the first term of Eq. (3) equals one. Here we account for the possibility of not being deep in the Lamb-Dicke confinement regime. In this case, and assuming a thermal distribution of modes,  $\langle \cos(\delta k \cdot \hat{z}_i) \rangle = \exp(-\delta k^2 \langle \hat{z}_i^2 \rangle / 2)$ . This factor is known as the Debye-Waller factor  $DWF$ . For our conditions all ions have approximately the same Debye-Waller factor,  $DWF \approx 0.86$  [3].

With  $\mu \sim \omega$ , Eq. (3) can be written as

$$\hat{H}_{ODF} = (U \cdot \delta k \cdot DWF) Z_c \cos((\omega - \mu)t + \delta - \phi) \sum_i \frac{\hat{\sigma}_i^z}{2}, \quad (4)$$

which is Eq. (2) of the main text with  $F_0 = U \cdot \delta k \cdot DWF$ .

## 2. LINESHAPE

To model the lineshape of the signal, it is necessary to account for the accumulated phase due to the spin-dependent ODF potential without making the simplification that  $\omega = \mu$ . This results in a characteristic response function for each sequence. For this Letter, we used an  $m = 8$  CPMG sequence, as shown in Fig. 1 in the main text and also Fig. 1 of this supplemental material. In the following, we derive the lineshape of this sequence using the modulation discussed in the first section and assuming a delta function source at a frequency  $\omega$ . This lineshape is used to generate the theory curves of Fig. 2 of the main text. In general, for a CPMG sequence it is necessary to calculate the phase evolution during  $2m$  terms of length  $T$ , for a total interaction time of  $2mT$ . For simplicity, we first derive the lineshape for the  $m = 2$  CPMG sequence (Fig. 1).

For a delta function source  $Z_c \cos(\omega t + \delta)$ , the spin precession accumulated in a general sequence like that shown in Fig. 1 is

$$\theta(\mu) = F_0 Z_c \frac{2 \sin\left(\frac{1}{2}(\omega - \mu)T\right)}{(\omega - \mu)} \chi(\mu, \omega), \quad (5)$$

where  $\chi(\mu, \omega) = \sum_i \chi_i(\mu, \omega)$  is determined by the particular sequence used. In the case of the  $m = 2$  CPMG sequence, the phase accumulated through four terms corresponding to four separate applications of the ODF (Fig. 1) must be considered:

$$\chi_1 = \cos\left[(\omega - \mu) \frac{T}{2} + \delta - \phi\right], \quad (6)$$

$$\chi_2 = -\cos\left[(\omega - \mu) \left(\frac{3T}{2} + t_\pi\right) + \delta - \phi + \mu(T + t_\pi)\right], \quad (7)$$

$$\chi_3 = -\cos\left[(\omega - \mu) \left(\frac{5T}{2} + t_\pi\right) + \delta - \phi + \mu(T + t_\pi)\right], \quad (8)$$



$$\chi_4 = \cos \left[ (\omega - \mu) \left( \frac{7T}{2} + 2t_\pi \right) + \delta - \phi + 2\mu(T + t_\pi) \right]. \quad (9)$$

Note these terms now include a phase  $\phi$  for the ODF interaction, which in the main text we set to zero with no loss of generality. Adding these terms up, pairwise:

$$\chi_1 + \chi_2 = 2 \sin \left( \frac{1}{2} [(\omega - \mu)(T + t_\pi) + \mu(T + t_\pi)] \right) \sin \left[ (\omega - \mu) \left( T + \frac{t_\pi}{2} \right) + \delta - \phi + \frac{\mu(T + t_\pi)}{2} \right], \quad (10)$$

$$\chi_3 + \chi_4 = -2 \sin \left( \frac{1}{2} [(\omega - \mu)(T + t_\pi) + \mu(T + t_\pi)] \right) \sin \left[ (\omega - \mu) \left( 3T + \frac{3t_\pi}{2} \right) + \delta - \phi + \frac{3\mu(T + t_\pi)}{2} \right]. \quad (11)$$

Summing all four terms yields

$$\chi(\mu, \omega) = \sum_i \chi_i(\mu, \omega) = 2 \sin \left( \frac{\omega}{2} (T + t_\pi) \right) [\sin(\xi + \delta - \phi) - \sin(3\xi + \delta - \phi)], \quad (12)$$

where  $\xi = (\omega - \mu)(T + \frac{t_\pi}{2}) + \frac{\mu(T + t_\pi)}{2} = \frac{1}{2} (\omega(T + t_\pi) + T(\omega - \mu))$ . Then, simplifying:

$$\chi(\mu, \omega) = 2 \sin \left( \frac{\omega}{2} (T + t_\pi) \right) 2 \sin(-\xi) \cos(2\xi + \delta - \phi). \quad (13)$$

Using Eqs. 13 and 5,

$$\theta(\mu) = DWF \cdot U \cdot \delta k \cdot Z_c \cdot T \operatorname{sinc} \left( \frac{T}{2} (\omega - \mu) \right) 4 \sin \left( \frac{\omega}{2} (T + t_\pi) \right) \sin(\xi) \cos(2\xi + \delta - \phi). \quad (14)$$

Since  $4T = \tau$  for the  $m = 2$  CPMG, then

$$\theta(\mu) = \theta_{max} \operatorname{sinc} \left( \frac{T}{2} (\omega - \mu) \right) \sin \left( \frac{\omega}{2} (T + t_\pi) \right) \sin(\xi) \cos(2\xi + \delta - \phi), \quad (15)$$

where  $\theta_{max} \equiv (F_0/\hbar) Z_c \tau$ , the maximum precession angle on resonance as defined in the main text. Then,  $\theta_{max}(\mu)$ , defined as  $\theta(\mu) = \theta_{max}(\mu) \cos(2\xi + \delta - \phi)$ , is the  $\mu$ -dependent generalization of  $\theta_{max}$ . From Eq. 15, this is

$$\theta_{max}(\mu) = \theta_{max} \operatorname{sinc} \left( \frac{T}{2} (\omega - \mu) \right) \sin \left( \frac{\omega}{2} (T + t_\pi) \right) \sin(\xi). \quad (16)$$

For the  $m = 8$  CPMG sequence the same procedure is used, but now with 16 periods of accumulated phase. We obtain

$$\theta_{max}(\mu) = \theta_{max} \operatorname{sinc} \left( \frac{T}{2} (\omega - \mu) \right) \sin \left( \frac{\omega}{2} (T + t_\pi) \right) \sin(\xi) \cos(2\xi) \cos(4\xi). \quad (17)$$

As shown in the main text, the expression for population in  $|\uparrow\rangle$  - now with a dependence on the ODF difference frequency  $\mu$  - is

$$\langle P_\uparrow \rangle = \frac{1}{2} [1 - e^{-\Gamma\tau} J_0(\theta_{max}(\mu))]. \quad (18)$$

Equations (17) and (18) are used to obtain the theoretical line shapes of Fig. (2) of the main text.

### 3. PHASE-INCOHERENT SENSING LIMITS

Here we derive Eq. (5) from the main text and provide additional mathematical background for the phase-incoherent experimental protocol, wherein the phase of the measured quadrature varies randomly from one realization of the experiment to the next. Following earlier discussions, the probability of measuring  $|\uparrow\rangle$  at the end of the Ramsey sequence is

$$\langle P_{\uparrow} \rangle = \frac{1}{2} [1 - e^{-\Gamma\tau} J_0(\theta_{max})] , \quad (19)$$

where  $\langle \rangle$  denotes an average over many experimental trials and therefore over the random phase between the 1D traveling-wave potential and the classically driven COM motion, and

$$\theta_{max} = (F_0/\hbar) \cdot Z_c \cdot \tau . \quad (20)$$

Defining  $G(\theta_{max}^2) \equiv (1 - J_0(\theta_{max}))/2$  and denoting  $\langle P_{\uparrow} \rangle_{bck} = [1 - e^{-\Gamma\tau}]/2$  as the probability of measuring  $|\uparrow\rangle$  at the end of the sequence in the absence of a classically driven motion,  $\theta_{max}^2$  can be determined from a measurement of the difference  $\langle P_{\uparrow} \rangle - \langle P_{\uparrow} \rangle_{bck}$  through

$$G(\theta_{max}^2) = e^{\Gamma\tau} (\langle P_{\uparrow} \rangle - \langle P_{\uparrow} \rangle_{bck}) . \quad (21)$$

The standard deviation  $\delta\theta_{max}^2$  in estimating  $\theta_{max}^2$  is determined from the standard deviation  $\sigma(P_{\uparrow} - P_{\uparrow,bck})$  of the  $\langle P_{\uparrow} \rangle - \langle P_{\uparrow} \rangle_{bck}$  difference measurements through

$$\delta\theta_{max}^2 = \frac{e^{\Gamma\tau} \sigma(\langle P_{\uparrow} \rangle - \langle P_{\uparrow} \rangle_{bck})}{\frac{dG(\theta_{max}^2)}{d\theta_{max}^2}} . \quad (22)$$

The signal-to-noise ratio of a measurement of  $\theta_{max}^2$  (and therefore  $Z_c^2$ ) is  $\theta_{max}^2/\delta\theta_{max}^2 = Z_c^2/\delta Z_c^2$ . In general this signal-to-noise ratio depends on  $\theta_{max}^2$  and the experimental parameters  $U \cdot \tau$ ,  $\Gamma \cdot \tau$ ,  $\delta k$ , and  $N$ .

We use Eq. (22) to theoretically estimate  $Z_c^2/\delta Z_c^2$  and the amplitude sensing limits. We assume the only sources of noise are projection noise in the measurement of the spin state and fluctuations in  $P_{\uparrow}$  due to the random variation in the relative phase of the 1D traveling-wave potential and the driven COM motion. Experimentally this is obtained by collecting 10 photons for each  $|\uparrow\rangle$  state, so photon counting shot noise can be neglected [3]. In this case  $\sigma(P_{\uparrow} - P_{\uparrow,bck}) = \sqrt{\sigma_{P_{\uparrow}}^2 + \sigma_{P_{\uparrow,bck}}^2}$  where the relevant variances are

$$\sigma_{P_{\uparrow,bck}}^2 = \frac{1}{N} \langle P_{\uparrow} \rangle_{bck} (1 - \langle P_{\uparrow} \rangle_{bck}) = \frac{1}{4N} (1 - e^{-2\Gamma\tau}) \quad (23)$$

and

$$\sigma_{P_{\uparrow}}^2 = \sigma_{\delta}^2 + \frac{1}{N} \langle P_{\uparrow} \rangle (1 - \langle P_{\uparrow} \rangle) . \quad (24)$$

Here  $N$  is the number of spins. Equation (23) and the second term in Eq. (24) are projection noise. The variance

$$\sigma_{\delta}^2 = \langle P_{\uparrow}^2 - \langle P_{\uparrow} \rangle^2 \rangle = \frac{e^{-2\Gamma\tau}}{8} (1 + J_0(2\theta_{max}) - 2J_0(\theta_{max})^2) \quad (25)$$

is due to the random variation in the relative phase of the 1D traveling-wave and the driven COM motion. For our set-up,  $DWF = \exp(-\delta k^2 \langle \dot{z}_i^2 \rangle / 2) = 0.86$  and  $\delta k = 2\pi/(900 \text{ nm})$  are fixed, the decoherence  $\Gamma$  is a function of  $U$ ,  $\Gamma = \xi(U/\hbar)$  where  $\xi = 1.156 \times 10^{-3}$ , and  $F_0 = DWF \cdot U \cdot \delta k$ . For a given  $Z_c$  we use Eqs. (20) and (22)-(25) to find the optimum  $Z_c^2/\delta Z_c^2$  as a function of  $(U\tau)/\hbar$ . This optimum value is the red dashed theoretical curve plotted in Fig. 4 of the main text.

The signal-to-noise  $Z_c^2/\delta Z_c^2$  is optimized for relatively small values of  $\theta_{max}^2$  where  $G(\theta_{max}^2) \approx \theta_{max}^2/8$  is a good approximation. This leads to some simplifications for Eqs. (21) and (22),

$$\theta_{max}^2 \approx 8e^{\Gamma\tau} (\langle P_{\uparrow} \rangle - \langle P_{\uparrow} \rangle_{bck}) \quad (26)$$

and

$$\delta\theta_{max}^2 \approx 8e^{\Gamma\tau} \sigma(P_{\uparrow} - P_{\uparrow,bck}) , \quad (27)$$

and to the following estimate for the signal-to-noise ratio of a single measurement,

$$\frac{\theta_{max}^2}{\delta\theta_{max}^2} = \frac{Z_c^2}{\delta Z_c^2} \approx \frac{\langle P_{\uparrow} \rangle - \langle P_{\uparrow} \rangle_{bck}}{\sigma(P_{\uparrow} - P_{\uparrow,bck})}. \quad (28)$$

Figure (4) of the main text uses Eq. (28), along with repeated measurements of  $P_{\uparrow} - P_{\uparrow,bck}$ , to experimentally determine the signal-to-noise ratio as a function of the imposed amplitude  $Z_c$  of the COM motion.

Finally we use Eqs. (20) and (22)-(25) to calculate the sensing limits for very small  $Z_c$ . For small  $Z_c$  the variance  $\sigma_{\delta}^2$  can be neglected compared to projection noise and  $\sigma_{P_{\uparrow}}^2 \approx \sigma_{P_{\uparrow,bck}}^2$ . In this case we obtain the following expression for the signal-to-noise ratio,

$$\frac{Z_c^2}{\delta Z_c^2} = \frac{\sqrt{N} DWF^2 \cdot (\delta k Z_c)^2 (U\tau/\hbar)^2}{4\sqrt{2} \sqrt{e^{2\xi U\tau/\hbar} - 1}}. \quad (29)$$

Equation (29) is maximized for  $\xi U\tau \approx 1.9603$ , resulting in

$$\left. \frac{Z_c^2}{\delta Z_c^2} \right|_{\text{limiting}} \approx 0.097 \frac{\sqrt{N} (DWF)^2 (\delta k)^2}{\xi^2} Z_c^2, \quad (30)$$

which is Eq. (5) of the main text. With  $DWF = 0.86$ ,  $\delta k = 2\pi/(900 \text{ nm})$ ,  $\xi = 1.156 \times 10^{-3}$ , and  $N = 85$ ,

$$\left. \frac{Z_c^2}{\delta Z_c^2} \right|_{\text{optimum}} = \left[ \frac{Z_c}{0.2 \text{ nm}} \right]^2. \quad (31)$$

For our set-up and available ODF power,  $\xi U\tau/\hbar \approx 1.9603$  is realized for  $\tau \approx 20 \text{ ms}$ . A measurement of the signal and a measurement of the background requires  $\sim 60 \text{ ms}$ , allowing for 16 independent measurements of  $P_{\uparrow} - P_{\uparrow,bck}$  in 1 s. The limiting sensitivity is approximately  $(100 \text{ pm})^2$  in a 1 s measurement time, or  $(100 \text{ pm})^2/\sqrt{\text{Hz}}$ . We note that the limiting sensitivity is determined by the ratio  $\xi = \Gamma/(U/\hbar)$ . In particular, the optimum value for Eq. (29) scales as  $1/\xi^2$ .

#### 4. PHASE-COHERENT SENSING LIMITS

With appropriate care the phase of the 1D traveling-wave potential can be stable for long periods of time with respect to the ion trapping electrodes [4], enabling repeated phase-coherent sensing of the same quadrature of the COM motion  $Z_c \cos(\omega t)$ . In this case the same spin precession  $\theta_{max} = DWF \cdot (U/\hbar) \cdot \delta k Z_c \cdot \tau$  occurs for each experimental trial, which can be detected to first order in  $\theta_{max}$  (or  $Z_c$ ) in a Ramsey sequence with a  $\pi/2$  phase shift between the two  $\pi/2$ -pulses. Assuming  $\sin(\theta_{max}) \approx \theta_{max}$ , appropriate for small amplitudes  $Z_c$ , the equivalent phase-coherent sensing expressions for Eqs. (26) and (27) are

$$\theta_{max} = 2e^{\Gamma\tau} (\langle P_{\uparrow} \rangle - \langle P_{\uparrow} \rangle_{bck}) \quad (32)$$

and

$$\delta\theta_{max} = 2e^{\Gamma\tau} \sigma(P_{\uparrow} - P_{\uparrow,bck}). \quad (33)$$

For a Ramsey experiment with a  $\pi/2$  phase shift,  $\langle P_{\uparrow} \rangle_{bck} = 1/2$ . If projection noise is the only source of noise, then for small  $Z_c$ ,  $\sigma_{P_{\uparrow}}^2 \approx \sigma_{P_{\uparrow,bck}}^2 = \frac{1}{N} \cdot \frac{1}{2} \cdot \frac{1}{2}$  and  $\sigma(P_{\uparrow} - P_{\uparrow,bck}) \approx \frac{1}{\sqrt{2N}}$ . The limiting signal-to-noise ratio  $\theta_{max}/\delta\theta_{max}$  of a  $(P_{\uparrow} - P_{\uparrow,bck})$  measurement is

$$\frac{\theta_{max}}{\delta\theta_{max}} = \frac{Z_c}{\delta Z_c} = DWF \cdot (\delta k Z_c) \cdot \sqrt{\frac{N}{2}} \cdot \frac{(U\tau)}{\hbar} e^{-\xi U\tau/\hbar}. \quad (34)$$

Equation (34) is maximized for  $\xi U\tau/\hbar = 1$ . With  $DWF = 0.86$ ,  $\delta k = 2\pi/(900 \text{ nm})$ ,  $\xi = 1.156 \times 10^{-3}$ , and  $N = 100$ ,

$$\left. \frac{Z_c}{\delta Z_c} \right|_{\text{optimum}} = \frac{Z_c}{0.074 \text{ nm}}. \quad (35)$$

With 16 independent measurements of  $\langle P_{\uparrow} \rangle - \langle P_{\uparrow} \rangle_{bck}$  in 1 s, this corresponds to a limiting sensitivity of  $\sim (20 \text{ pm})/\sqrt{\text{Hz}}$ . The optimum value for the signal-to-ratio of Eq. (34) scales as  $1/\xi$ . By employing spin-squeezed states that have been demonstrated in this system [3],  $Z_c/\delta Z_c$  can be improved by another factor of 2.

Employing this technique to sense motion on resonance with the COM mode can lead to the detection of very weak forces and electric fields. The detection of a 20 pm amplitude resulting from a 100 ms coherent drive on the 1.57 MHz COM mode is sensitive to a force/ion of  $5 \times 10^{-5} \text{ yN}$ , corresponding to an electric field of 0.35 nV/m.

---

\* kevin.gilmore@colorado.edu

† john.bollinger@nist.gov

- [1] S. Kotler, N. Akerman, Y. Glickman, A. Keselman, and R. Ozeri, *Nature* **473**, 61 (2011).
- [2] J. W. Britton, B. C. Sawyer, A. C. Keith, C.-C. J. Wang, J. K. Freericks, H. Uys, M. J. Biercuk, and J. J. Bollinger, *Nature* **484**, 489 (2012) (see Supplementary Information).
- [3] J. G. Bohnet, B. C. Sawyer, J. W. Britton, M. L. Wall, A. M. Rey, M. Foss-Feig, and J. J. Bollinger, *Science* **352**, 1297 (2016) (see Supplementary Information).
- [4] D. B. Hume, C. W. Chou, D. R. Leibbrandt, M. J. Thorpe, D. J. Wineland, and T. Rosenband, *Physical Review Letters* **107**, 243902 (2011).